Nuclear Medicine and Biology 138-139 (2024) 108962

Contents lists available at ScienceDirect

Nuclear Medicine and Biology

journal homepage: www.elsevier.com/locate/nucmedbio

Longitudinal multimodal monitoring of transplanted islet β-cells

Filippo C. Michelotti [a], Gregory Bowden [a], Wael Eter [b], Astrid Küppers [c], Andreas Maurer [a], Volker Nischwitz [c,1], Bernd J. Pichler [a], Martin Gotthardt [b], Andreas M. Schmid [a,*]

[a] Werner Siemens Imaging Center, Department of Preclinical Imaging and Radiopharmacy, Eberhard Karls University Tübingen, Tübingen, Germany
[b] Radboud University Nijmegen Medical Centre, Department of Radiology Nuclear Medicine, Nijmegen, the Netherlands
[c] Forschungszentrum Jülich GmbH, Central Institute of Engineering, Electronics and Analytics, Jülich, Germany

ARTICLE INFO

Keywords:
PET/MRI
Transplanted islets
Manganese
GLP-1R
LA-ICP-MS imaging

ABSTRACT

Purpose: Monitoring β-cell mass and function would provide a better understanding of diabetes, setting the stage for truly individualized therapies. We applied a combined PET/MRI protocol to monitor engrafted islets mass and function without pre-labeling of isolated cells. A PET tracer binding to GLP-1R quantifies β-cell mass, while Mn-CA characterizes β-cell function. Both parameters were assessed in transplanted and native β-cells *in vivo* and validated with autoradiography and mass spectrometry imaging.

Methods: Islets were collected and transplanted into the calves of C3H-mice. Accumulation of [^{64}Cu]Ex4 and Mn-CA was examined with a PET/MRI at 1 h post-injection between 1 and 4 weeks after the transplantation. A separate blocking study with diazoxide targeted the functionality of the transplanted islets. As validation, *ex vivo* autoradiography and LA-ICP-MS imaging were performed after the last imaging session.

Results: PET/MRI monitored the engraftment of transplanted islets and visualized an increasing uptake of the PET tracer and Mn-CA. The Mn-CA accumulated at a higher islet-to-background ratio in the calf of mice than in the pancreas due to the high retention of Mn-CA in the exocrine pancreas. *In vivo* imaging data correlated well with autoradiography and LA-ICP-MS imaging, validating the *in vivo* approaches.

Conclusion: For the quantification of β-cell function, Mn-based contrast mechanisms between native and transplanted islets differ and require further studies for optimal biological readout. However, non-invasive PET/MRI nonetheless provides the tools to investigate the relationship between β-cell mass and function in pancreatic islets.

1. Introduction

An auto-immune response against the insulin-secreting β-cells is a key hallmark of type 1 diabetes mellitus [1]. It has been long hypothesized that with most of the β-cells depleted, these patients lose the capacity to produce and secrete insulin and require life-long treatment with exogenous insulin. However, novel findings suggest that the size of the residual pool of viable β-cells in some individuals might be underestimated and that β-cell dysfunction may play a hitherto underestimated role in type 1 diabetes. The established methods, such as serum C-peptides measures and insulin staining, may not be able to detect residual β-cells [2,3]. Thus, a method for non-invasive detection of viable but dysfunctional β-cells might have a significant impact on our understanding of the pathophysiology of type 1 diabetes [4,5].

Besides measuring viable β-cell mass in the pancreas, detection of islet grafts is another important task for improving therapy of type 1 diabetes. Among other available medical interventions, islet transplantation has the potential to replace or complement the long-term administration of insulin in patients with type 1 diabetes. However, due to functional failure of the islet grafts over time and the requirement of immunosuppression, this method is only used in selected individuals to improve glycemic control in individuals with frequent hypoglycemia even if insulin independence is not maintained. Current research aims to develop novel methods and strategies to prolong the functionality and survival of engrafted islet β-cells in the long-term [6]. Therefore, the development of a reliable, quantifiable, and non-invasive technique to

* Corresponding author at: Röntgenweg 13, 72074 Tuebingen, Germany.
E-mail addresses: Filippo.Michelotti@ddz.de (F.C. Michelotti), Gregory.Bowden@med.uni-tuebingen.de (G. Bowden), Wael.ArabiEter@radboudumc.nl (W. Eter), as.kueppers@fz-juelich.de (A. Küppers), Andreas.Maurer@med.uni-tuebingen.de (A. Maurer), volker.nischwitz@hswt.de (V. Nischwitz), Bernd.Pichler@med.uni-tuebingen.de (B.J. Pichler), Martin.Gotthardt@radboudumc.nl (M. Gotthardt), A.Schmid@med.uni-tuebingen.de (A.M. Schmid).
[1] Current Address: Weihenstephan-Triesdorf University of Applied Sciences, Department Environmental Engineering, Weidenbach, Germany.

https://doi.org/10.1016/j.nucmedbio.2024.108962
Received 5 August 2024; Received in revised form 18 September 2024; Accepted 3 October 2024
Available online 4 October 2024

monitor the efficacy of novel therapies *in vivo* is a sought-after tool by diabetologists. Here, several imaging methods have emerged as promising tools to assess the viability of grafted islets.

Nuclear imaging techniques employ radiolabeled exendin-derivatives to quantify β-cell mass *in vivo* by binding to glucagon-like-peptide 1 (GLP-1) receptors [4]. Recently, this approach allowed monitoring the engraftment of intramuscular islets until 6 weeks post-transplantation using single photon emission computed tomography (SPECT) [7]. Other methods, such as magnetic resonance imaging (MRI) and positron emission tomography (PET), also provide approaches to allow the longitudinal monitoring of engrafted islets [8].

By pre-labeling isolated cells with different contrast agents, MRI enables *in vivo* tracking of these cells [8]. Despite the high sensitivity of super-paramagnetic MRI probes, the gradual release of the contrast agent following cell death impedes the modality's ability to monitor the fate of engrafted islets in the mid/long-term [9,10].

A more specific approach, beyond cell-tracking, aims at quantifying β-cell function. Leoni et al. showed *in vitro* that β-cells internalize paramagnetic manganese (Mn) ions through the voltage-dependent calcium channels (VDCC) upon insulin secretion [11].

In a combined approach, using ^{64}Cu-labeled exendin-4 ([^{64}Cu]Ex4) PET and Mn-enhanced MRI allows non-invasive assessment of β-cell mass and function independently. This potentially provides a spatially resolved function-per-mass readout separating healthy clusters from viable but dysfunctional cells. Furthermore, the combined PET/MRI protocol revealed that pancreatic islets incorporate Mn-contrast agent (Mn-CA) at increased levels compared with surrounding tissue only after the gradual wash-out by the exocrine pancreas [12].

Thus, here we investigated a simultaneous PET/MRI approach to monitor the engraftment of transplanted islets. In combination, this PET/MRI method has potential to provide a simultaneous quantitative readout of β-cell mass and function. The specific internalization of the PET tracer and Mn-CA was validated through *in vivo* blocking of VDCC. Further, *ex vivo* analysis of pancreatic and transplanted islets by autoradiography and laser ablation-inductively coupled plasma-mass spectrometry (LA-ICP-MS) imaging correlated the specific localization of tracer uptake and Mn-CA.

2. Research design and methods

2.1. Radiolabeling of [^{64}Cu]NODAGA-40Lys-Exendin-4

[^{64}Cu]$CuCl_2$ (100 MBq in 0.01 HCl) was produced as described previously [13] and neutralized with 1.5× its volume ammonium acetate buffer (0.5 M, pH 6) that had been pretreated with Chelex 100 resin (4.6 g/200 mL). This solution was complemented with 4 μg NODAGA40Lys-Exendin-4 (Peptide Specialty Laboratories, Heidelberg, Germany) in deionized water (1 μg/ μl). After mixing, the solution was incubated at 42 °C for 20 min. RadioTLC (Polygram Sil G/UV254) run using a citrate buffer (0.1 M, pH 5) as the mobile phase was used to determine the labeling efficiency of the reaction (typically 90–95 % with <2 % free ^{64}Cu). The reaction solution was formulated for injection with PBS buffer (pH 7.4) 0.1 % Tween 20 *v*/v to a final volume of 400 μL. A final injecting volume of 50 μL was prepared using NaCl at ~106.7 GBq/μmol of molar activity.

2.2. Transplanted C3H mouse model

All animal experiments were carried out in accordance with the German Animal Welfare Law and after approval by the responsible local authorities. Littermate 6–7 wk-old male C3H mice (Charles River, Sulzfeld, Germany) were divided into the respective donor and recipient cohorts (3:1 ratio) and allowed one week to adapt. The islet transplantation procedure was performed as per the published protocol [7]. Briefly, before the surgery, a series of 50 mL Falcon tubes were filled with Roswel Park Memorial Institute (RPMI) 1640, 0.9 mg/mL collagenase-V solution (Sigma Aldrich, St Louis, MO, USA) and kept in ice. After euthanizing the animals, a volume of 2–3 mL of collagenase solution was injected through the bile duct. The collected pancreata were incubated for ~10–12 min at 37 °C in TW20 water bath (Julabo GmbH, Seelbach, Germany). The digestion was stopped by filling the tubes with cold RPMI 1640 medium, 10 % fetal calf serum, 100 penicillin units/mL, streptomycin 100 μL/mL. The pellet was collected, washed twice with fresh medium, and filtered with a 500 μm mesh. The resulting filtered solution was transferred into 50 mL Falcon tubes filled with fresh medium. After centrifugation, the resulting pellet was separated by gently adding 15 mL of each Ficoll solution (Cellgro by Mediatech Inc., Manassas, VA, USA) in the order 1.118, 1.096, and 1.037 g/mL and centrifugated at 1900 RPM for 16 min without brake.

The islets between the first and the second layer were hand-picked with a micropipette and transferred to a 15 mL falcon tube. After centrifugation at 600 RPM for 2 min, the islets were resuspended and counted in a 96-well plate by taking a volume of 40 μL mixed with 40 μL of trypan blue.

For the inoculation of islets into the calve muscles, ~600 islets per mouse were hand-picked and resuspended in a volume of ~30 μL.

2.3. Experimental workflow

After transplantation of ~600 islet cells, C3H mice (n = 3) were monitored with a PET/MRI protocol until 4 weeks post-inoculation. A mixture of $MnCl_2$:Bicine solution was freshly prepared before the start of the experiment using manganese(II) chloride tetrahydrate and bicine (Sigma-Aldrich Chemie GmbH, Germany). Following the induction of anesthesia, mice were i.v. injected with a stimulating glucose dose (1.5 g/kg; 50 μL). Serial bolus injections of 50 μL of [^{64}Cu]Ex4 (~0.12 MBq/g) and $MnCl_2$:Bicine (~75 μmol/kg) injecting solutions were administered five minutes after glucose stimulation. After an uptake time of ~1 h, 20 min-static PET scans were acquired. Subsequently, the animal bed was transferred to a 7 T small animal MRI scanner (Bruker BioSpin MRI GmbH, Ettlingen, Germany). The calves of the mice were centered for the acquisition of a T_1 map. After the last imaging time point, the animals were sacrificed. The radioactivity of the calf muscles, including the transplanted islets, and the contralateral control muscles, were measured by *ex vivo* γ-counting.

In the blocking study, two separated cohorts (n = 5/5) of age-matched littermate C3H mice were assessed with an analogous protocol 5 weeks after the inoculation of islets. The mice were pre-treated either by injecting 50 μL of diazoxide solution (23 mg/kg), previously dissolved in NaCl solution 0.1 M NaOH, or the same volume of vehicle solution. After 7 min, two volumes of 50 μL of [^{64}Cu]Ex4 (~0.12 MBq) and $MnCl_2$:Bicine solution (~75 μmol/kg) were injected through the same tail vein catheter. Subsequently, both groups, treated and control, received a stimulation dose of glucose (1.5 g/kg) 30 min after the contrast agent. After *in vivo* measurements, *ex vivo* autoradiography and LA-ICP-MS imaging were performed on the sections of the pancreas and the transplanted islets in the muscle, that were visible from the *in vivo* PET measurements.

2.4. PET acquisition

Following the induction of anesthesia, mice were placed in the center of the FoV of a dedicated small animal PET scanner (Inveon DPET, Siemens Healthineers, Knoxville, TN, USA) [14,15]. PET data was acquired for 20 min and reconstructed using a 3D ordered-subsets-expectation-maximization algorithm (OSEM3D-fastMAP) with the following parameters: MAP-subsets = 16, MAP-iteration = 18, OSEM3D-iteration = 2, 256 × 256 × 159 of matrix size and voxel size 0.388 × 0.388 × 0.796 mm^3. Subsequently, the animal was transferred to the MRI scanner.

2.5. MRI acquisition

Mouse calf muscles were centered in the field of view. Subsequently, consecutive 3D-FLASH protocols with different flip angles (TR/TE = 10/1.9 ms, FoV = 34 × 34 × 17 mm3, matrix size 128 × 128, NA = 2, BW = 75 kHz, FAs = 4° and 22°, isotropic resolution 0.3 mm) were used for analysis.

2.6. Γ-counter and Biodistribution

After the *in vivo* measurements, the muscle containing the transplanted islets and the contralateral control muscle of the calf, as well as the pancreas, liver, spleen, kidneys, and colon, were collected in dedicated γ-counter tubes (Sardstedt AG & Co., Nümbrecht, Germany). A set of standard vials was measured as a reference to quantify the radioactivity in the organs. The vials were weighed before and after the transfer of the tissues using a precision scale (Sartorius, Göttingen, Germany). The counts were measured using a Wallac 1480 WIZARD 3″ γ-counter (Perkin Elmer, Waltham, MA, USA) and decay corrected for ^{64}Cu ($T_{1/2}$ = 12.7 h). The signal was normalized for the injected activity and the tissue weights to calculate the organ-specific uptake of the PET tracer.

2.7. Autoradiography

After cervical dislocation was performed under anesthesia, the pancreata and the muscle containing the transplanted islets were embedded in optimum cutting temperature embedding compound (O.C.T., Sakura, Zoeterwonde, Netherlands) and snap-frozen at −20 °C. Cryosections (20 μm) were obtained using a Cryostat (Leica 1850, Leica GmbH, Wetzlar, Germany). The slides were exposed to a 35 × 43 cm^2 Storage Phosphor Screen (445SI, Molecular Dynamics, Sunnyvale, CA, USA) for 12 h. Autoradiography data was acquired using a dedicated phosphor scanner (STORM 840, Amersham Biosciences, Amersham, UK) at a spatial resolution of 50 × 50 μm^2. Autoradiography analysis was performed using ImageJ (US NIH, Bethesda, Maryland, USA) [16]. Regions of interest were drawn in the pancreatic and transplanted islets and the surrounding exocrine pancreas and muscle for reference, respectively. Mean values were extracted and used for statistical analysis.

2.8. LA-ICP-MS imaging

Subsequently to autoradiography, the slides were air-dried and scanned line-by-line with a 60 μm laser spot size using a laser ablation system (NWR 213, New Wave Research, Fremont, CA, USA). The aerosol of the ablated tissue was transported *via* an argon gas flow through a transfer line to an ICP-MS (Agilent 7900, Agilent Technologies, Santa Clara, California, USA), analyzing the isotopes ^{44}Ca, ^{65}Cu, ^{64}Zn, ^{55}Mn, and ^{13}C. Image reconstruction was performed *via* an in-house software package IMAGENA [17]. The 8-bit elemental images of ^{44}Ca (red channel), ^{64}Zn (green channel), and ^{55}Mn (blue channel) were merged by additive colour model.

2.9. Statistical analysis

Prism 9.2.0 (GraphPad Software, San Diego, Ca, USA) was used for statistical analysis. A one-sample Student's *t*-test was performed to determine the significance between the quantification of tracer uptake and relaxivity in log(%ID/mL) and log(R_1), respectively, between the muscle containing the transplanted islets and its contralateral control. The comparison between the group treated with diazoxide and the control group was performed by a two-sample Student's t-test assuming unequal variance between the groups using 0.05 as the Alpha level.

3. Results

3.1. Longitudinal evaluation of engrafted islet cells until four weeks after transplantation

In the first study, PET/MRI visualized the engraftment of ~600 transplanted islets in the calves of CH3 mice (n = 3) 1, 3, and 4 weeks after the transplantation. Images were acquired 1 h after the co-injection of the Mn-CA and PET tracer. Single hot-spot regions within the calf of the transplanted legs suggested that the engrafted islets had efficiently internalized both PET tracer and Mn-CA three weeks after transplantation on a representative mouse (Fig. 1A). Analysis of longitudinal images revealed a slight increase over time in both uptake of the PET tracer and Mn-CA accumulation (Fig. 1B, C), respectively.

The PET tracer biodistribution study showed the kidneys to have the highest uptake values with a mean tracer uptake of 36.0 ± 3.8 %ID/g, followed by liver and pancreas, with 6.6 ± 0.2 %ID/g and 4.3 ± 0.3 %ID/g, respectively (Fig. 1D). In direct comparison, tracer uptake in the calf muscle containing the transplanted islet cells was significantly higher than in the contralateral tissue (t(2.0) = 11.92, $^*p$ = 0.007), with values reaching 0.4 ± 0.1 %ID/g. It is worth to mention that the actual tracer uptake is underestimated due to the presence of muscle tissue with low tracer uptake within the relevant voxels.

3.2. Blocking of VDCC activity of islet transplant monitored in vivo using a combined PET/MR imaging setup

On a separate group of mice with transplanted cells, a blocking dose of diazoxide (23 mg/kg) was administered 7 min before the co-injection of the tracers. Co-localization of the PET tracer and Mn-CA was validated by autoradiography and LA-ICP-MS imaging (Fig. 2A). Static PET/MRI measurements of the calves were performed at 5 weeks after the transplantation on the treated and control groups of mice. One measurement was discarded due to the movement of the animal during the acquisition, while two animals did not show tracer uptake in the transplants in PET imaging. The comparison of animals showing visible PET uptake in the engrafted islets (n = 4/3) resulted in slight differences between the respective groups for the tracer uptake (t(3.9) = 0.3, p = 0.75) and Mn uptake (t(3.1) = 1.0, p = 0.39), respectively (Fig. 2B, C). The R_1 values of engrafted islets in the control group were slightly higher than in the treated group.

After the *in vivo* measurements, *ex vivo* autoradiography and LA-ICP-MS imaging of the pancreata and the transplanted calf sections were performed sequentially (Fig. 2A). In agreement with the *in vivo* results, single hot-spots with high endogenous levels of ^{44}Ca and ^{64}Zn were identified within the transplanted calf sections (Fig. 2D, E and Table 1). The contrast and the spatial distribution of ^{44}Ca and ^{64}Zn agreed well with ^{55}Mn. Areas at high concentrations of calcium and zinc indicate the presence of viable and active engrafted islet cells. Compared to the control group, the islets-to-muscle ratio calculated from the elemental images of ^{44}Ca, ^{55}Mn, and ^{64}Zn were slightly higher in the group of mice treated with diazoxide (Table 1).

Compared with the elemental images of the divalent ions, the levels of ^{13}C and ^{65}Cu were homogeneously distributed throughout the entire muscle and did not show any difference with the engrafted islets.

3.3. Ex vivo analysis of native pancreatic islets after VDCC blocking

Similarly, PET tracer and Mn-CA accumulation within the native pancreatic β-cells was also analyzed. Islet-to-background ratios were substantially lower in the pancreas due to the low background signal of muscle tissue (< 1 %ID/g) and the comparably high uptake of radiotracer by the exocrine pancreas of mice. Contrast and spatial distribution of ^{44}Ca and ^{64}Zn and the specific accumulation of the PET tracer (autoradiography) were inversely related to ^{55}Mn, revealing the presence of several hot-spots scattered throughout the pancreas sections,

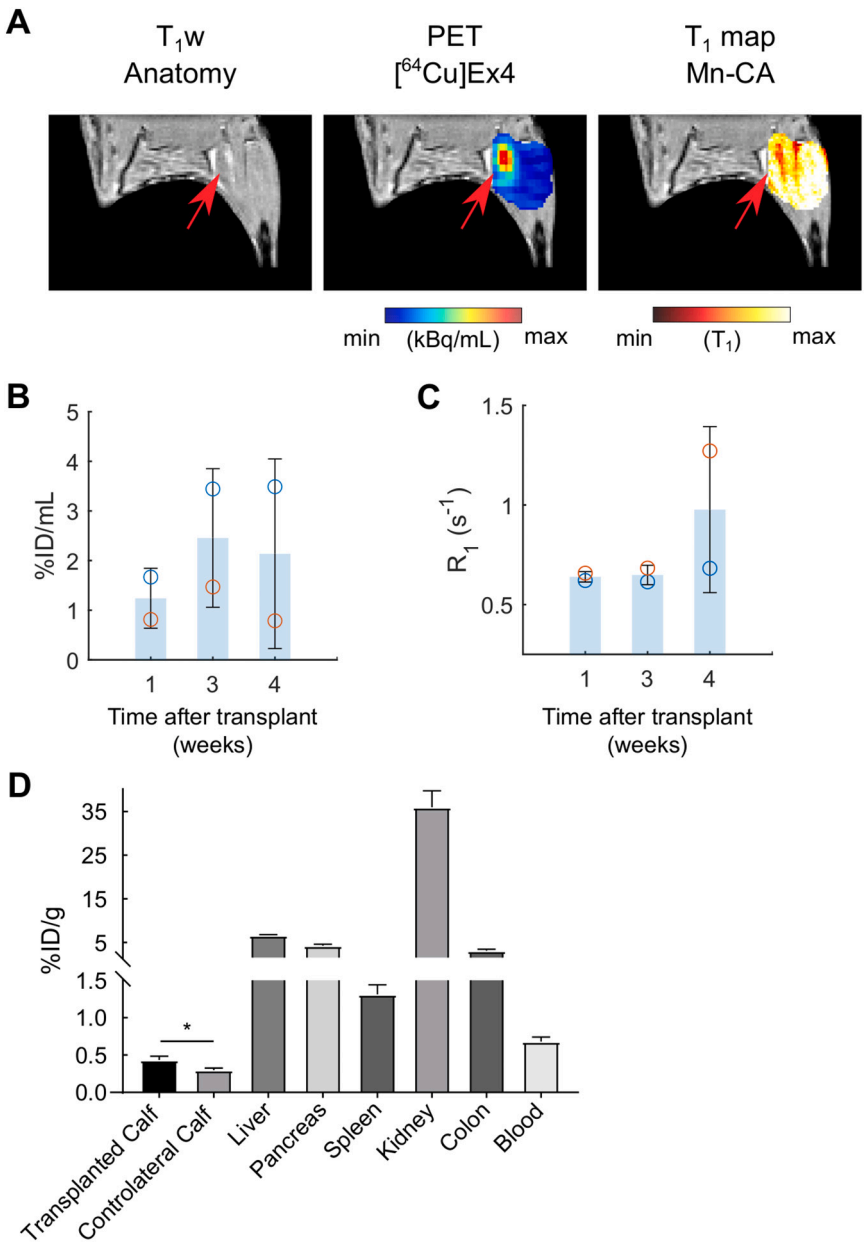

Fig. 1. Longitudinal PET/MRI of engrafted islets (1–4 weeks)
(A) Anatomical Mn-enhanced T_1-w images are used as a reference for the respective PET images and T_1 maps of ~600 islets (red arrow) 3 weeks post-transplantation in the right upper calf. (B) [^{64}Cu]Ex4 uptake and (C) Mn-CA update between 1 and after 4 weeks post-transplantation of ~600 islets. The circles indicate values from individual animals. (D) *Ex vivo* biodistribution of [^{64}Cu]Ex4 in the organs of interest, values are shown as mean ± SD. One-sample Student's *t*-test was performed to assess the difference between the uptake of the contralateral and transplanted calf. (For interpretation of the references to colour in this figure legend, the reader is referred to the web version of this article.)

corresponding to the pancreatic islets (Fig. 3). The islet-to-background ratios of transplanted and pancreatic islets were comparable for calcium and zinc, while manganese showed high background uptake in the exocrine pancreas.

4. Discussion

A central aspect of this study was the possibility to monitor β-cell mass and function simultaneously and elucidate differences in the physiological behavior of native and engrafted β-cell islets. Our data and literature [7] show that the revascularization of islets occurs between 1 and 3 weeks and correlates with a gradual increase of radiolabeled exendin uptake, which remains stable until the last imaging session post-transplantation of our study.

Analysis of volumetric ME-MR images co-registered with PET also shows an increased Mn accumulation during the islet engraftment, suggesting that the islets' insulin secretory capacity might recover during revascularization.

Once internalized in the intracellular space, manganese ions are readily sequestered from the cytosol in different sub-cellular compartments, including the nucleus, mitochondria, and endoplasmic reticulum [18]. In our studies, each animal received a single administration of $MnCl_2$ at low doses (75 μmol/kg) immediately before the imaging session.

Beyond *in vivo* PET/MRI, our findings were further validated by combining autoradiography and LA-ICP-MS imaging analysis on the same tissue slice. *Ex vivo* imaging of ^{55}Mn and the comparison with the natural abundance of ^{44}Ca and ^{64}Zn allowed for the quantification of

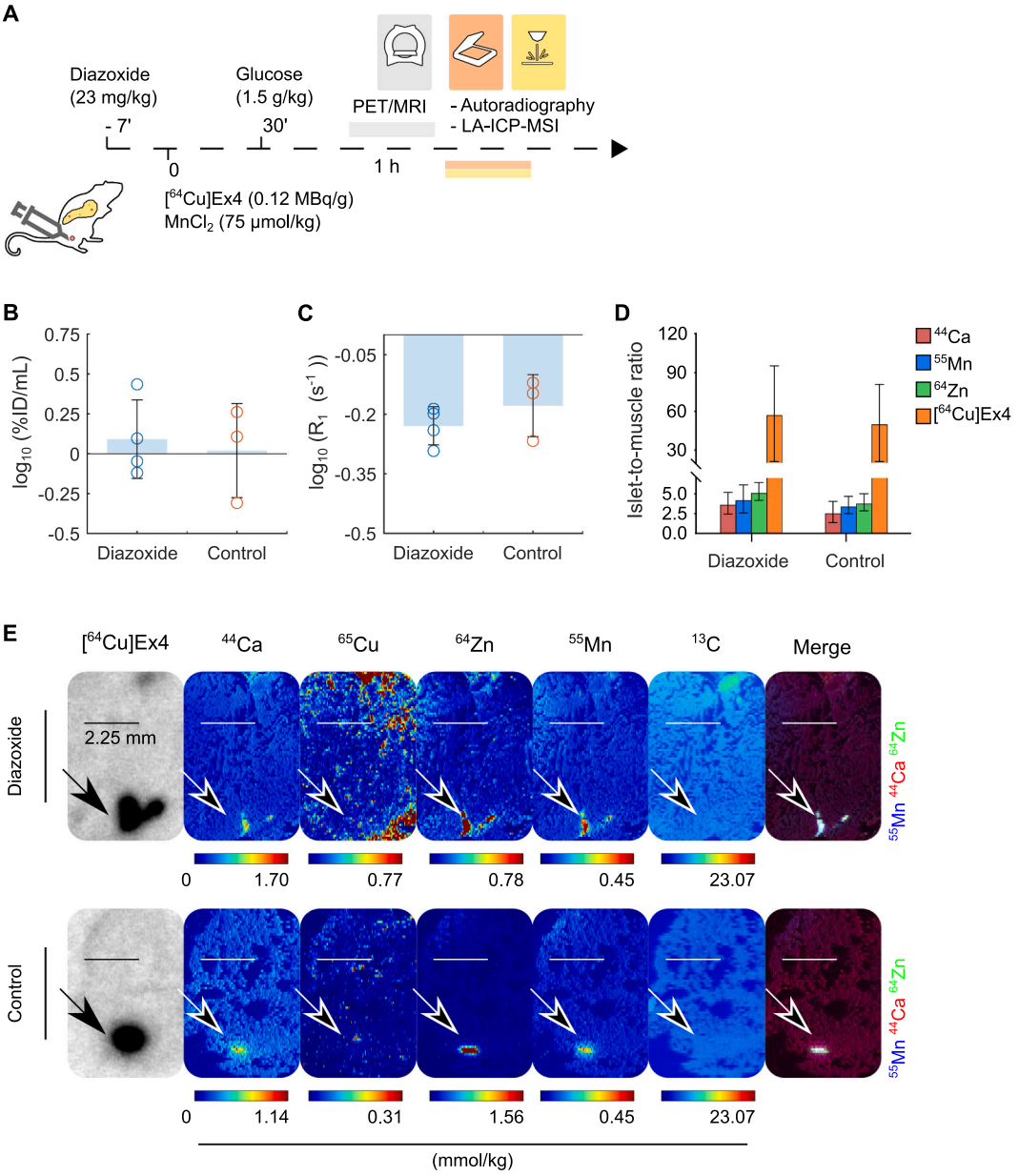

Fig. 2. PET/MRI quantification and *ex vivo* analysis revealed specific accumulation of probes in the transplanted calf
(A) Schematic representation of the blocking study performed at 5 weeks after the transplantation of ~600 islets. The bar charts show the uptake of (B) [^{64}Cu]Ex4 (log(%ID/mL)) and (C) Mn (log(R_1($^{s-1}$))) in calf of transplanted mice in the control (red circles) and treated group (blue circles) ($n = 4/3$). Differences in PET tracer uptake ($t(3.9) = 0.3$, $p = 0.75$) and quantitative maps of T_1 ($t(3.1) = 1.0$, $p = 0.39$) between control and treated animals are calculated by a two-sample Student's *t*-test. (D) The islet-to-muscle ratio calculated from the autoradiography of the PET tracer ([^{64}Cu]Ex4) and from the elemental images (^{44}Ca, ^{55}Mn, and ^{64}Zn) of the same muscle sections are shown for treated and control groups ($n = 2/2$). (E) The black arrows indicate the single spots at high signal-to-background localized in the calf sections (dark spot) and with high levels of ^{44}Ca and ^{64}Zn images compared to ^{13}C and ^{65}Cu images. Scale bars are set to 2.25 mm. Merged elemental images show the co-localization of endogenous metals and exogenous ^{55}Mn (white spot) in both control and treated mice. (For interpretation of the references to colour in this figure legend, the reader is referred to the web version of this article.)

Table 1
Ex vivo quantification of transplanted islets.

	LA-ICP-MS imaging			Autoradiography
Group	**^{44}Ca**	**^{55}Mn**	**^{64}Zn**	**[^{64}Cu] Ex4**
Diazoxide	3.8 ± 1.4	4.4 ± 1.8	5.3 ± 1.1	58.1 ± 37.1
Control	2.7 ± 1.3	3.6 ± 1.1	3.9 ± 1.1	51.0 ± 29.9

Islet-to-muscle ratios calculated from the elemental images (^{44}Ca, ^{55}Mn and ^{64}Zn) and autoradiography of exendin ([^{64}Cu]Ex4) of the calf of control and treated mice. Values are presented as mean ± SD.

trace amounts of Mn-CA in the native pancreatic islets and engrafted islets at high spatial resolution. This approach relies on the high turnover of calcium and zinc ions related to insulin production, storage, and secretion in β-cells [19]. Interestingly, contrast and spatial distribution of ^{55}Mn were comparable to ^{44}Ca and ^{64}Zn. This indicates that Mn-CA is actively internalized as a divalent cation analog in the intracellular space of the engrafted islet cells.

Furthermore, we targeted the internalization of Mn in a separate group of mice treated with a blocking dose of diazoxide (23 mg/kg). The hyperglycemic effect of diazoxide is mediated by inhibiting VDCC activity through the binding and opening of ATP-sensitive potassium

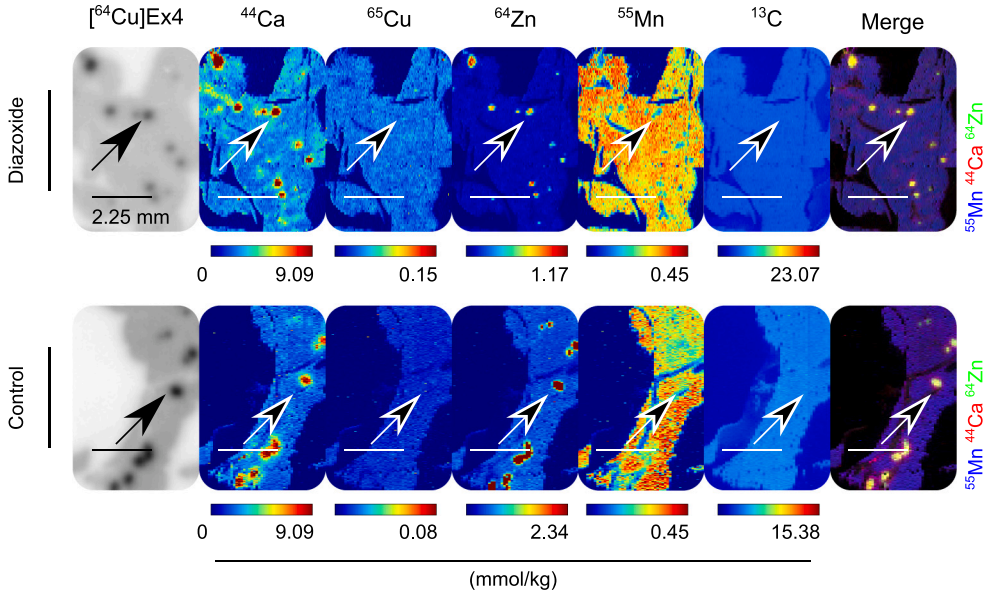

Fig. 3. *Ex vivo* analysis of pancreas identifies unspecific accumulation of exogenous Mn in the exocrine pancreas
The black arrows indicate the diffuse hot-spots at high levels of ^{44}Ca and ^{64}Zn and the accumulation of the PET tracer (dark spots) throughout the pancreas sections of control and mice pre-treated with diazoxide. Scale bars are set to 2.25 mm. Merged elemental images show the specific co-localization of ^{44}Ca and ^{64}Zn (yellow spots), in contrast to the high accumulation of ^{55}Mn in the surrounding exocrine areas throughout the pancreas sections in both control and treated groups. (For interpretation of the references to colour in this figure legend, the reader is referred to the web version of this article.)

channels. In this regard, our experimental setup did not detect a significant change in Mn uptake from the group of mice treated with diazoxide before glucose stimulation, although the reduced R_1 values in the treatment group suggest a partial blocking of the VDCC activity and Mn internalization from the engrafted islets. However, a slight increase in the levels of divalent ions within the pancreatic islets was observed from the *ex vivo* analysis, which might be linked to a reduction of the basal secretory insulin response in the diazoxide-treated animals.

Previous studies showed that challenges with high diazoxide doses could inhibit the insulin response to glucose *in vivo* and in perfused rat pancreata [20]. However, in the same experiments, the incubation of diazoxide before glucose stimulation, such as in our experimental setup, led to an augmented response to glucose. Thus, further elucidation of the effects of diazoxide would be necessary to link the internalization of Mn and insulin response in this mouse model.

In agreement with previous findings [12], high perfusion and binding of Mn to the exocrine pancreas impaired the visualization of pancreatic islets. The estimated concentration of Mn in the exocrine pancreas at 1 h post-injection was around twice the amount measured in the pancreatic islets.

By contrast, the accumulation of the PET tracer in the pancreatic islets was three times higher than in the exocrine pancreas despite mouse-strain-specific, receptor-mediated uptake in the exocrine pancreas [21]. A direct comparison between the PET tracer and Mn-CA is not feasible as they have different molecular targets. However, these findings have important implications for the development of novel Mn-based imaging methods in combination with PET using radiolabeled GLP-1 to obtain direct indexes of β-cell mass and function [10,22].

Improving the sensitivity of Mn-imaging methods could measure the fraction of Mn retained in the intracellular compartments of the islets [11,12]. This, however, requires alternative imaging protocols with low toxicity and a complete wash-out of un-specifically bound contrast agent. Alternatively, carrier systems could be developed to avoid the excessive accumulation of Mn-CA in off-target tissues, such as in the brain [23].

In addition to evaluating the pathophysiology of type 1 diabetes and characterizing islet transplants, combined PET/MR imaging of β-cell function and mass may also help answer current questions in type 2 diabetes. A first proof-of-principle study was carried-out to monitor the engraftment of intrahepatic islets using radiolabeled exendin in patients with type 1 diabetes [24]. Another study showed that Mn-based imaging techniques holds promises in the evaluation of the pancreas of type 1 diabetes [25]. Our method may provide a spatially resolved function-per-mass readout to discriminate healthy engrafted islets from viable but dysfunctional islets.

In clinical research, recent clustering studies using estimates of β-cell function and insulin resistance have proposed the presence of different endotypes of diabetes groups, each sharing different risks for the development of diabetes-related complications [26,27]. Their clinical relevance is currently discussed [28]. Evaluating the distribution of β-cell mass and function among those subgroups might be important. Deriving β-cell mass and function directly through non-invasive imaging may allow further refinement of these clustering approaches. Localized function-per-mass readout could improve tailored therapies by adapting therapy schemes for certain patients to the actual propensity to produce/secrete insulin or to better use the functional capacity of existing but dysfunctional β-cells.

Regarding the translation of methods, previous studies have shown that high exposure of Mn could cause cytotoxic side effects in certain brain areas and other endocrine tissues [23]. In our studies, each animal received a single administration of $MnCl_2$ at low doses (75 μmol/kg) immediately before the imaging sessions. Thus, further studies would be necessary to evaluate the potential side effects of repeated administrations of Mn-CA on the viability of engrafted islets. However, the increasing accumulation of [^{64}Cu]Ex4 and Mn-CA into the β-cells over time does not allude to significant cytotoxic effects on the transplanted islets. By improving the sensitivity of Mn-based imaging methods it will be possible measure the fraction of Mn retained in the intracellular compartments of the islets.

5. Conclusion

A combined PET/MRI approach allows the simultaneous detection and monitoring of engrafted and pancreatic β-cells in their host

environment. Using radiolabeled GLP-1 agonists and paramagnetic Mn-CA provides a quantitative readout of the secretory capacity per islet and could improve patient stratification. However, further refinement of the imaging protocol for clinically relevant application will be required.

CRediT authorship contribution statement

Filippo C. Michelotti: Writing – review & editing, Writing – original draft, Visualization, Validation, Software, Methodology, Investigation, Formal analysis, Data curation, Conceptualization. **Gregory Bowden:** Writing – review & editing, Writing – original draft, Methodology, Formal analysis. **Wael Eter:** Validation, Methodology. **Astrid Küppers:** Methodology, Formal analysis. **Andreas Maurer:** Writing – review & editing, Supervision, Project administration. **Volker Nischwitz:** Writing – review & editing, Resources, Methodology. **Bernd J. Pichler:** Writing – review & editing, Supervision, Resources, Project administration, Funding acquisition. **Martin Gotthardt:** Writing – review & editing, Writing – original draft, Supervision, Project administration, Funding acquisition. **Andreas M. Schmid:** Writing – review & editing, Writing – original draft, Supervision, Project administration, Conceptualization.

Declaration of competing interest

Bernd J. Pichler has research collaborations with MEDISO, Hungary, on the development of small animal PET/MR and with Siemens on MR compatible PET electronics and breast PET/MR. Martin Gotthardt is a co-inventor of a patent on exendin.

Acknowledgments

We thank Sandro Aidone, Maren Harant, and Natalie Mucha for valuable technical assistance. The authors would like to thank Prof. Reischl and the Radiopharmacy Tuebingen for providing the ^{64}Cu. This work is part of the Ph.D. thesis of F.C.M.

Author contributions

A.M.S., A.M., M.G., and B.J.P. supervised and discussed the progress of research. F.C.M., A.M.S., M.G., and B.J.P. designed the experiments and wrote the manuscript. F.C.M. carried out the experiments and analyzed the data. G.B. established and performed the radiolabeling of the PET tracer. A.K. and V.N. performed mass spectrometry imaging of biometals. W.E. carried out the experiments for the isolation and transplantation of islets at our facility. All authors corrected and reviewed the manuscript. M.G. coordinated the BetaTrain Consortium.

Guarantor statement

A.M.S. is the guarantor of this work and, as such, had full access to all the data in the study and takes responsibility for the integrity of the data and the accuracy of the data analysis.

Funding source

This research received funding from the European Research Council under the European Union's Seventh Framework Programme (FP7/2007–2013) grant agreement n° 289,932 BetaTrain and the Werner Siemens Foundation (Zug, Switzerland).

References

[1] Quattrin T, Mastrandrea LD, Walker LSK. Type 1 diabetes. Lancet 2023;401 (10394):2149–62. https://doi.org/10.1016/S0140-6736(23)00223-4.

[2] Oram RA, Sims EK, Evans-Molina C. Beta cells in type 1 diabetes: mass and function; sleeping or dead? Diabetologia 2019;62(4):567–77. https://doi.org/10.1007/s00125-019-4822-4.

[3] Marselli L, et al. Are we overestimating the loss of beta cells in type 2 diabetes? Diabetologia 2014;57(2):362–5. https://doi.org/10.1007/s00125-013-3098-3.

[4] Eriksson O, et al. In vivo imaging of beta cells with radiotracers: state of the art, prospects and recommendations for development and use. Diabetologia 2016;59 (7):1340–9. https://doi.org/10.1007/s00125-016-3959-7.

[5] Gurzov EN, Ke PC, Ahlgren U, Garcia Ribeiro RS, Gotthardt M. Novel strategies to protect and visualize pancreatic β cells in diabetes. Trends Endocrinol Metab 2020; 31(12):905–17. https://doi.org/10.1016/j.tem.2020.10.002.

[6] M. R. Rickels and R. P. Robertson, "Pancreatic islet transplantation in humans: recent Progress and future directions," Endocr Rev, vol. 40, no. 2, pp. 631–668, Apr. 2019, doi:https://doi.org/10.1210/er.2018-00154.

[7] Eter WA, Bos D, Frielink C, Boerman OC, Brom M, Gotthardt M. Graft revascularization is essential for non-invasive monitoring of transplanted islets with radiolabeled exendin. Sci Rep 2015;5(1):15521. https://doi.org/10.1038/srep15521.

[8] N. Sakata *et al.*, "Imaging of transplanted islets by positron emission tomography, magnetic resonance imaging, and ultrasonography," Islets, vol. 5, no. 5, pp. 179–187, Sep. 2013, doi:https://doi.org/10.4161/isl.26980.

[9] M. L. Malosio *et al.*, "MR imaging monitoring of Iron-labeled pancreatic islets in a small series of patients: islet fate in successful, unsuccessful, and autotransplantation," Cell Transplant, vol. 24, no. 11, pp. 2285–2296, Nov. 2015, doi:https://doi.org/10.3727/096368914X684060.

[10] Wei W, Ehlerding EB, Lan X, Luo Q-Y, Cai W. Molecular imaging of β-cells: diabetes and beyond. Adv Drug Deliv Rev 2019;139:16–31. https://doi.org/10.1016/j.addr.2018.06.022.

[11] L. Leoni, S. D. Serai, R. L. Magin, and B. B. Roman, "Functional MRI characterization of isolated human islet activation," NMR Biomed, vol. 23, no. 10, pp. 1158–1165, Dec. 2010, doi:https://doi.org/10.1002/nbm.1542.

[12] Michelotti FC, et al. PET/MRI enables simultaneous in vivo quantification of β-cell mass and function. Theranostics 2020;10(1):398–410. https://doi.org/10.7150/thno.33410.

[13] C. M. Griessinger *et al.*, "64Cu antibody-targeting of the T-cell receptor and subsequent internalization enables in vivo tracking of lymphocytes by PET," Proc Natl Acad Sci, vol. 112, no. 4, pp. 1161–1166, Jan. 2015, doi:https://doi.org/10.1073/pnas.1418391112.

[14] Kemp BJ, Hruska CB, McFarland AR, Lenox MW, Lowe VJ. NEMA NU 2-2007 performance measurements of the Siemens Inveon™ preclinical small animal PET system. Phys Med Biol 2009;54(8):2359. https://doi.org/10.1088/0031-9155/54/8/007.

[15] Mannheim JG, et al. Quantification accuracy and partial volume effect in dependence of the attenuation correction of a state-of-the-art small animal PET scanner. Phys Med Biol 2012;57(12):3981. https://doi.org/10.1088/0031-9155/57/12/3981.

[16] Schneider CA, Rasband WS, Eliceiri KW. NIH image to ImageJ: 25 years of image analysis. Nat Methods 2012;9(7):671–5. https://doi.org/10.1038/nmeth.2089.

[17] Osterholt T, Salber D, Matusch A, Becker JS, Palm C. IMAGENA: image generation and analysis – an interactive software tool handling LA-ICP-MS data. Int J Mass Spectrom 2011;307(1):232–9. https://doi.org/10.1016/j.ijms.2011.03.010.

[18] L. Leoni, A. Dhyani, P. La Riviere, S. Vogt, B. Lai, and B. B. Roman, "β-Cell subcellular localization of glucose-stimulated Mn uptake by X-ray fluorescence microscopy: implications for pancreatic MRI," Contrast Media Mol Imaging, vol. 6, no. 6, pp. 474–481, Nov. 2011, doi:https://doi.org/10.1002/cmmi.447.

[19] J. C. Hou, L. Min, and J. E. Pessin, "Chapter 16 Insulin Granule Biogenesis, Trafficking and Exocytosis," in *Vitamins & Hormones*, vol. 80, Academic Press, 2009, pp. 473–506. doi:https://doi.org/10.1016/S0083-6729(08)00616-X.

[20] I. M. Burr, E. B. Marliss, W. Stauffacher, and A. E. Renold, "Diazoxide effects on biphasic insulin release: 'adrenergic' suppression and enhancement in the perifused rat pancreas," J Clin Invest, vol. 50, no. 7, pp. 1444–1450, Jul. 1971, doi:https://doi.org/10.1172/JCI106628.

[21] Willekens SMA, et al. Strain differences determine the suitability of animal models for noninvasive in vivo Beta cell mass determination with radiolabeled Exendin. Mol Imaging Biol 2016;18(5):705–14. https://doi.org/10.1007/s11307-016-0936-y.

[22] Chen C, Cohrs CM, Stertmann J, Bozsak R, Speier S. Human beta cell mass and function in diabetes: recent advances in knowledge and technologies to understand disease pathogenesis. Mol Metab 2017;6(9):943–57. https://doi.org/10.1016/j.molmet.2017.06.019.

[23] A. C. Silva, J. H. Lee, I. Aoki, and A. P. Koretsky, "Manganese-enhanced magnetic resonance imaging (MEMRI): methodological and practical considerations," NMR Biomed, vol. 17, no. 8, pp. 532–543, Nov. 2004, doi:https://doi.org/10.1002/nbm.945.

[24] M. Gotthardt, L. Joosten, T. J. P. Jansen, M. Brom, M. Boss, and S. M. A. Willekens, "From mice to men: the exocrine pancreas does not matter for human GLP-1 receptor imaging," J Nucl Med, p. jnumed.120.259184, Feb. 2021, doi:https://doi.org/10.2967/jnumed.120.259184.

[25] S. S. Joshi *et al.*, "Non-invasive imaging of functional pancreatic islet beta-cell mass in people with type 1 diabetes mellitus," Diabet Med, vol. 40, no. 10, p. e15111, Oct. 2023, doi:https://doi.org/10.1111/dme.15111.

[26] Ahlqvist E, et al. Novel subgroups of adult-onset diabetes and their association with outcomes: a data-driven cluster analysis of six variables. Lancet Diabetes Endocrinol 2018;6(5):361–9. https://doi.org/10.1016/S2213-8587(18)30051-2.
[27] Zaharia OP, et al. Risk of diabetes-associated diseases in subgroups of patients with recent-onset diabetes: a 5-year follow-up study. Lancet Diabetes Endocrinol 2019;7(9):684–94. https://doi.org/10.1016/S2213-8587(19)30187-1.
[28] Dennis JM, Shields BM, Henley WE, Jones AG, Hattersley AT. Disease progression and treatment response in data-driven subgroups of type 2 diabetes compared with models based on simple clinical features: an analysis using clinical trial data. Lancet Diabetes Endocrinol 2019;7(6):442–51. https://doi.org/10.1016/S2213-8587(19)30087-7.